ACS APPLIED MATERIALS & INTERFACES

Research Article

www.acsami.org

# Directing Vascular Cell Selectivity and Hemocompatibility on Patterned Platforms Featuring Variable Topographic Geometry and Size

Yonghui Ding,[†] Zhilu Yang,[⊥] Cathy W. C. Bi,[‡] Meng Yang,[†] Sherry Li Xu,[‡] Xiong Lu,[⊥] Nan Huang,[⊥] Pingbo Huang,[‡,§,∥] and Yang Leng*[,†]

[†]Department of Mechanical and Aerospace Engineering, [‡]Division of Life Science, [§]Division of Biomedical Engineering, and [∥]State Key Laboratory of Molecular Neuroscience, The Hong Kong University of Science and Technology, Clear Water Bay, Kowloon, Hong Kong

[⊥]Key laboratory of Advanced Technology of Materials, School of Material Science and Engineering, Southwest Jiaotong University, Chengdu, 610031 Sichuan, China

Supporting Information

**ABSTRACT:** It is great challenge to generate multifunctionality of vascular grafts and stents to enable vascular cell selectivity and improve hemocompatibility. Micro/nanopatterning of vascular implant surfaces for such multifunctionality is a direction to be explored. We developed a novel patterned platform featuring two typical geometries (groove and pillar) and six pattern sizes (0.5−50 $\mu$m) in a single substrate to evaluate the response of vascular cells and platelets. Our results indicate that targeted multifunctionality can be indeed instructed by rationally designed surface topography. The pillars nonselectively inhibited the growth of endothelial and smooth muscle cells. By contrast, the grooves displayed selective effects: in a size-dependent manner, the grooves enhanced endothelialization but inhibited the growth of smooth muscle cells. Moreover, our studies suggest that topographic cues can affect response of vascular cells by regulating focal adhesion and stress fiber development, which define cytoskeleton organization and cell shape. Notably, both the grooves and the pillars at 1 $\mu$m size drastically reduced platelet adhesion and activation. Taken together, these findings suggest that the topographic pattern featuring 1 $\mu$m grooves may be the optimal design of surface multifunctionality that favors vascular cell selectivity and improves hemocompatibility.

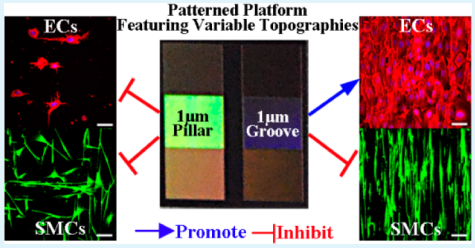


**KEYWORDS:** *surface topography, vascular cells, hemocompatibility, multifunctionality*

## 1. INTRODUCTION

Vascular stents or grafts are commonly used for treating coronary artery disease. However, such implantations are associated with major complications such as in-stent restenosis caused by the proliferation of vascular smooth muscle cells (SMCs) and thrombosis induced by inadequate re-endothelialization on the surface and poor hemocompatibility of the vascular devices. Thus, in developing next-generation vascular devices, the aim is to favor rapid endothelialization while concomitantly inhibiting high SMC proliferation ("vascular cell selectivity") and improving hemocompatibility.

Numerous factors at the cell−substrate interface are known to affect cellular adhesion, spreading, proliferation, and other functions.[1] Among these factors, surface topography is a critical parameter that directs vascular cell fates and platelet adhesion/activation.[2−5] Interactions of vascular cells with the topographic features on surfaces varies with topographic geometry, feature size and cell type; however, no general principle appears to apply when predicting how vascular cells may respond to surface topography. Matrix anisotropy has been shown to potentially improve the functions of endothelial cells (ECs), such as induce enhanced EC migration[2] and an athero-resistant phenotype,[3] by generating in-vivo-like EC alignment. However, the effect of anisotropic patterns on EC proliferation remains debated.[2,4,5] Furthermore, matrix anisotropy restricts SMC spreading in a single direction, which results in SMC becoming elongated and proliferating at low rates.[6−8] Moreover, the effects of the isotropic features of the matrix on the behavior of vascular cells remain ambiguous: whereas certain studies have suggested that ECs adhered and spread more efficiently on an isotropic pillar-patterned surface than they do on a flat surface,[9,10] one study demonstrated the opposite result.[11] Recently, a surface featuring submicrometer pillars was reported to reduce platelet adhesion and activation when compared with a flat surface.[12−14] Notably, few studies have focused on concurrently directing the behaviors of ECs, SMCs, and platelets on surfaces featuring topographic patterns, let alone on clearly identifying the optimal topography (geometry and size) that endows surfaces with such multifunctionality. Therefore, the influence of topographic features on vascular

Received: February 21, 2014
Accepted: July 21, 2014
Published: July 21, 2014

cell selectivity and hemocompatibility warrants further investigation.

To attain the aforementioned goal, reliable results must be obtained on the vascular cell selectivity and hemocompatibility of topographic patterns over a large scale of topographic geometries and feature sizes. However, such large-scale screening is not feasible because the screening is expensive, time-consuming, and experimentally unreliability. Recently, combinatorial sample formats such as microarray polymer libraries and orthogonal-gradient sample formats designed for high-throughput screening of cell−surface interactions have been developed.[15−18] Incorporating high-throughput techniques can facilitate rapid, large-scale screening of topographies and their interactions with vascular cells. However, studies on topographic effects on cells should include a sufficient size of individual topographic motifs in a microarray to ensure that the evaluations are highly reliable; otherwise, given the tens of micrometers size range of cells, unequivocal visual and statistical assessment of cell behavior would be challenging.

In this work, we developed a novel patterned platform consisting of 12 topographic motifs (4.5 × 2.9 $mm^2$ each) including two typical geometries, anisotropic grooves and isotropic pillars, and six feature sizes ranging from 0.5 to 50 $\mu$m (spanning across the single-cell size). Using this platform, we performed highly efficient and reliable evaluations of EC, SMC, and platelet responses to variable topographies. This experimental setup allows quick and accurate identification of optimal topographic geometry and feature size that can potentially endow surfaces with multifunctionality and thus favor EC growth and concomitantly inhibit SMC proliferation and platelet adhesion/activation.

## 2. EXPERIMENTAL SECTION

**2.1. Fabrication of Patterned Platform.** The patterned platform was first fabricated on silicon wafers through standard photolithography and deep reactive-ion etching (DRIE). We designed a novel patterned platform in which a single substrate contains an array of 2 × 6 motifs (4.5 × 2.9 $mm^2$ each) and each motif has a unique arrangement of patterns that vary in topographic geometry (groove and pillar) and feature size (0.5−50 $\mu$m); we used a flat area as the control (Figure 1A). As shown in Figure 1A, the patterned motifs are named G (groove) or P (pillar) and the numbers shown after the letters represent the size in micrometers; for example, G1 represents a groove pattern that is 1 $\mu$m in size. The patterned silicon substrate was

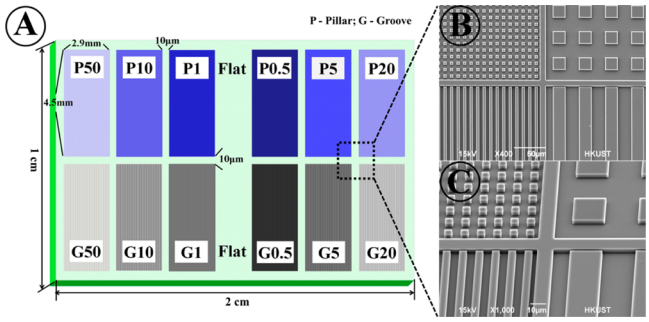


**Figure 1.** (A) Schematic of patterned platform consisting of 2 × 6 motifs (~4.5 mm × 2.9 mm each) separated by a 10 $\mu$m wide wall as well as flat surface control, and each motif contains a unique pillar (P) or groove (G) varying in size (width = spacing = 0.5, 1, 5, 10, 20, 50 $\mu$m). (B) Top-view and (C) tilted-view (ca. 75°) of SEM images taken from the dashed box labeled in (A) show four adjacent motifs on patterned platform.

then coated with a thin layer of titanium by using a radio frequency (RF) sputtering system (model Explorer 14, Denton Vacuum). A post-sputtering heat treatment was conducted at 700 °C for 1 h under an air flow to transfer the coating layer to the titanium oxide.

**2.2. Vascular Cell Culture.** Human umbilical vein endothelial cells (HUVECs) were isolated from human umbilical vein.[19] Briefly, the human umbilical vein was filled with 0.1% collagenase II and incubated at 37 °C for 15 min. The digestion was stopped by adding M199 medium (Hyclone) with 15% fetal bovine serum (FBS, Hyclone). HUVECs were collected by centrifugation of the digested cell suspension. The harvested HUVECs were cultured in 0.2%-gelatin-coated T75 flasks with Lonza Endothelial Growth Medium (EGM) bullet kit containing 100 U/mL penicillin and 100 U/mL streptomycin in a humidified incubator with 95% air and 5% $CO_2$. HUVECs between passages 2 and 7 were used for experiments to ensure the genetic stability of the cultures. HUVECs were plated on the patterned platforms at a density of 7500 cells/$cm^2$ and incubated for various periods (2 h, 1 day, or 3 days).

Human umbilical artery smooth muscle cells (HUASMCs) were obtained through the slow outgrowth of the cells from small pieces of umbilical artery in media, and were cultured in DMEM/F12 medium containing 10% FBS. The culture medium was changed every 3 days. The cells were subcultured when >80% confluent, and the cells were used in experiments between passages 2 and 5. HUASMCs were plated on the patterned platforms at a density of 1.5 × $10^4$ cells/$cm^2$ and incubated for the same periods as the HUVECs.

**2.3. HUVEC Attachment, Proliferation, and Morphology Analysis.** Cell attachment was evaluated based on cell numbers on the patterns after 2 h incubations. Cell proliferation was determined by measuring the increase in cell numbers from day 1 to 3 in culture. To perform these evaluations, HUVECs cultured on the patterned platforms were fixed with 4% paraformaldehyde (PFA; Sigma-Aldrich) in phosphate buffered saline (PBS) for 20 min at room temperature. The cells were then permeabilized using 0.5% Triton X-100 in PBS for 5 min and blocked with 1% bovine serum albumin (BSA; Sigma-Aldrich) in PBS for 60 min to reduce nonspecific staining. Subsequently, to examine cytoskeletal formation, the cells were labeled for F-actin by using phalloidin conjugated to tetramethyl rhodamine isothiocyanate (TRITC) (2 $\mu$g/mL; Sigma-Aldrich) for 60 min at room temperature. The cells were also counter-stained with DAPI (1 $\mu$g/mL; Sigma-Aldrich) to image nuclei. To examine the focal adhesions (FAs) in HUVECs, the cells were first stained with monoclonal anti-human vinculin antibodies (no. ab18058, 1:50 dilution; Abcam, Cambridge, U.K.) overnight at 4 °C. After washing with PBS, the cells were incubated for 60 min with goat polyclonal secondary antibodies against mouse IgG (H&L, FITC-linked; no. ab6785, 1:500 dilution; Abcam). The samples were finally washed three times in PBS and mounted on microscope slides for examination using confocal laser scanning microscopy (LSM710, Zeiss, Germany).

**2.4. Cell Viability of HUVECs.** Cell viability of adherent HUVECs was assessed using a cell-permeable Calcein-AM (Life Technologies, Inc., NY) in combination with a plasma membrane-impermeable DNA-binding dye propidium iodide (PI, Sigma-Aldrich) after 1 day of culture. The cells were stained with a 1:1 mixture of Calcein-AM (2 $\mu$g/mL) and PI (50 $\mu$g/mL) at 37 °C for 20 min, and then immediately inspected in a fluorescence microscope.

**2.5. Determination of HUVEC Phenotype.** We used immunostaining to analyze the expression of two key endothelial cell markers: platelet endothelial cell adhesion molecule (PECAM-1/CD31) and von Willebrand factor (vWF). HUVECs were plated on the patterned platforms at a density of 2.5 × $10^4$ cells/$cm^2$. After 1 day incubation, the cells were fixed with 4% PFA in PBS, permeabilized using 0.5% Triton X-100, blocked with 1% BSA, treated with primary antibodies overnight at 4 °C, incubated with secondary antibodies for 60 min at room temperature, and finally counter-stained with DAPI. Antibodies were used at the following dilutions: 1:20 for monoclonal mouse anti-human CD31 antibody (Dako, Copenhagen, Denmark), 1:200 for polyclonal rabbit anti-human vWF antibody (Dako), and 1:500 for FITC-linked goat polyclonal secondary antibodies against mouse IgG.

**2.6. Evaluations of HUASMCs and Platelets.** HUASMCs were identified by immunostaining with rat anti-human $\alpha$-smooth muscle actin ($\alpha$-SMA) primary antibodies and FITC-labeled sheep anti-rat IgG. The protocol used to evaluate platelet adhesion has been described in our previous report.[14] Briefly, to prepare platelet-rich plasma (PRP), whole blood was centrifuged (200g, 15 min) and the supernatant was collected. The PRP (50 $\mu$L) was placed on the sample surfaces and incubated at 37 °C for 2 h. After washing in PBS, the samples were prepared for examination using scanning electron microscopy (SEM).

**2.7. Scanning Electron Microscopy.** The morphology of cells and platelets on the patterned platforms was examined using SEM (JSM-6390, JEOL, Japan). After various periods in culture, the cells were fixed with 2.5% glutaraldehyde for 1 h. The platforms were rinsed three times with PBS and then dehydrated using an ethanol series (30%, 50%, 75%, 90%, and 100%; 15−30 min each), and subsequently maintained in 100% ethyl alcohol until drying. The patterned platforms were dried overnight in a vacuum chamber and then mounted on copper stubs and sputter-coated with gold before SEM examination.

**2.8. Image Analysis.** Immunostained images were analyzed with ImageJ (National Institutes of Health). Cell counts were analyzed by using the "Analyze particles" tool in ImageJ. For quantitation of cell morphology, the cell profile was manually drawn using the "Freehand selections" tool, and an ellipse was fitted to the cell profile by using the "Fit ellipse" options in the "Measurement" tool. The angle between the major ellipse axis and the image $y$-axis, that is, the direction of groove alignment, was measured and defined as the cell alignment angle. Furthermore, cell shape parameters such as the projected area per cell and the cell elongation (minor/major axis ratios) were determined by ImageJ. For quantitation of the number of FAs per cell, the image was converted to 8 bit, and threshold was adjusted automatically by "Adjust threshold" tool. After that, the number of FAs was counted by the "Analyze particles" tool.

**2.9. Statistical Study.** At least three substrates were used for each assay, and all assays were repeated in triplicate. All data are expressed as mean ± standard deviation (SD). One-way analysis of variance (ANOVA) test was used to measure differences for experiments with multiple data sets with a post hoc Tukey multiple comparison test performed between groups with significant differences. A value of $p \leq 0.05$ was considered statistically significant.

## 3. RESULTS

**3.1. Fabrication of Patterned Platform.** The patterned platforms featuring an array of 2 × 6 distinct motifs of topographic patterns on a single silicon chip were fabricated as shown in Figure 1B and C. A fence-like structure with a 10 $\mu$m space between two motifs was designed to minimize the possibility of adjacent motifs affecting cell behavior. SEM examinations revealed that all the topographic patterns exhibited highly regular geometric features and a uniform height of 3.5 $\mu$m. The formation of a thin film of titanium oxide was confirmed by performing cross-sectional SEM examination and thin-film X-ray diffraction analysis, as described by us in detail elsewhere.[14]

**3.2. HUVEC Responses.** *3.2.1. Attachment, Proliferation, Morphology, and Viability.* The attachment of HUVECs on various topographic patterns was evaluated after culturing the cells for 2 h (Figure 2A). Comparing cell densities on surfaces featuring one specific pattern geometry (either groove or pillar) but variable pattern sizes revealed a biphasic trend: the cell density was proportional to pattern sizes between 0 (flat surface) and 1 $\mu$m, but inversely proportional to pattern size when the pattern size was 5 $\mu$m or larger. This trend was clearer on the groove patterns than on the pillars. Furthermore, the cell density was higher on grooves than on pillars of the same size, and this disparity in cell density between the grooves and pillars

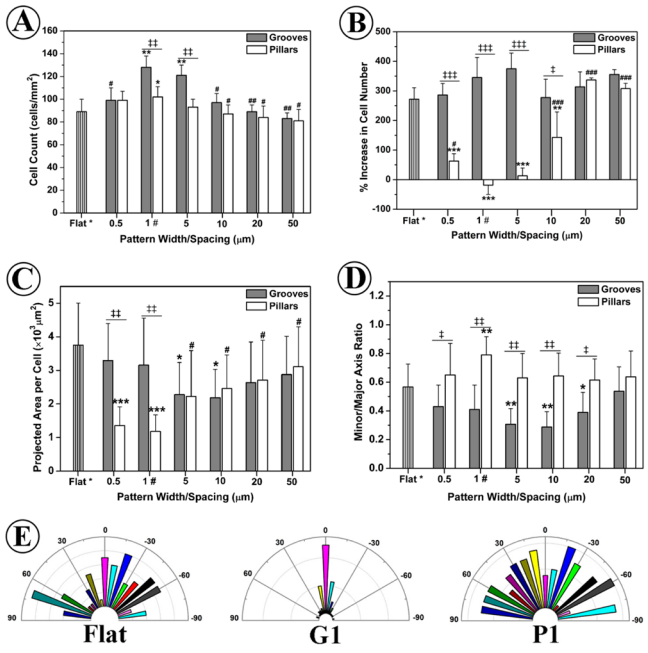


**Figure 2.** Analysis of EC attachment, proliferation, and morphology on various patterned surfaces. (A) The cell density of ECs attached onto the surfaces after culturing cells for 2 h was analyzed from at least 12 images of each patterned motif. (B) The proliferation rate of ECs was represented by relative increase in cell number from day 1 to 3 in culture. (C) Projected area per cell, (D) minor/major axis ratios, and (E) distribution of cell alignment angles measured as the angle between cell orientation and groove direction (oriented nominally at 0°) were calculated from at least 120 cells from six different images of each pattered motif after culturing cells for 1 day. Statistically significant differences are marked as follows: * vs flat surface; # vs G1 for grooves or P1 for pillars; ‡ same-sized groove vs pillar.

reached a maximal value of ∼30% at a pattern size of 1 $\mu$m. We also noted that the cell densities on three patterns, G1, G5, and P1, were substantially higher than that on the flat surface.

The proliferation rate of HUVECs was analyzed by determining the relative changes in cell density from day 1 to 3 in culture (Figure 2B and Supporting Information Figure S1). For a given pattern size, proliferation rates were considerably higher for the cells cultured on the grooves and on the flat surface compared with those on the pillars. These proliferation rates were more distinct on small-sized patterns (especially G1 vs P1), but the difference diminished on large-sized patterns (i.e., 20 and 50 $\mu$m). The proliferation rate appeared to be independent of groove size, although these rates were slightly higher on G1 and G5 than on other groove patterns. By contrast, the proliferation rate showed a typical biphasic dependence of pillar size: the rate decreased 10-fold from P10 to P5 and reached the lowest level on P1 and then increased by 4.5-fold on the submicrometer pillar P0.5. These results indicated that the proliferation of HUVECs depends intricately on both pattern geometry and size. Geometry markedly affected proliferation only when the pattern size was 10 $\mu$m or less, and the effect maximized around 1 $\mu$m, but then diminished at 0.5 $\mu$m. The effect of size was stronger with pillars than with grooves.

Next, SEM studies revealed that HUVECs attached to various surfaces in 2 h cultures exhibited distinct morphologies (Figure 3): attached HUVECs were closely aligned and polarized along the groove direction on the grooves, whereas

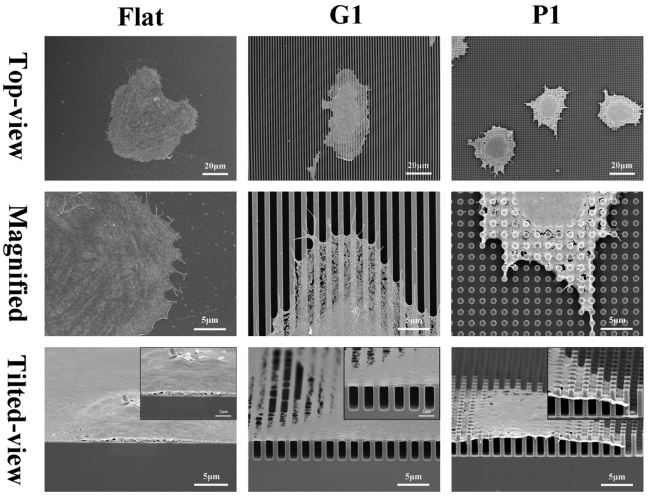


**Figure 3.** Top-view, magnified top-view, and tilted-view (*z*-sectioning, ca. 75°) of SEM images of ECs on the surfaces of Flat, G1, and P1 after culturing cells for 2 h.

they were small and round on the pillars and rounded and spread out on the flat surface. Intriguingly, compared with P1, the G1 and the flat surfaces promoted greater cell spreading, although large numbers of cellular protrusions and filopodia were observed on all the surfaces. Moreover, titled-views of z-sectioned substrates showed that the cells on the flat surface were flattened and attached to the surfaces through the entire cell body as expected, whereas the cells on the G1 surface attached exclusively to the top of the ridges and the cells spanned several ridges. Notably, the cells showed similar bridging over pillars on P1, but the cell bodies gradually sagged from the center to cell periphery; in this case, the side-walls of the pillars may have hindered the extension of cell protrusions and thereby suppressed cell spreading.

To further evaluate the cellular spreading and cytoskeletal formation in HUVECs cultured on the patterned platforms, F-actin and nuclei were examined using fluorescence microscopy (Figures 4 and S2). Projected area per cell was first quantified after culturing cells for 1 day (Figure 2C). All patterned surfaces appeared to suppress cell spreading compared with the flat surface: P0.5 and P1 inhibited cell spreading most strongly, whereas G0.5 and G1 displayed the weakest inhibitory effect. Next, we quantified the time course of the change in projected cell area on the flat surface, G1, and P1 (Figure S3B). Interestingly, the projected cell area first increased from 2 h to 1 day in culture and then decreased sharply (by 40%−60%) after 3 days of culture on the flat surface and G1. By contrast, the projected cell area was smaller on P1 than on other surfaces and it changed little over the entire culture period. These observations suggested that the G1 and flat surfaces promoted cell spreading and therefore cell division, whereas the P1 surface strongly suppressed cell spreading and division. This notion was further supported by the cell area coverage being substantially higher on the G1 and flat surfaces than on P1 after 1 day in culture (Figure S3A). Notably, cultured HUVECs became fully confluent in 3 days on the G1 and flat surfaces, but they were less than 10% confluent on the P1 surface (Figure 4) and the number of cells on P1 appeared to decrease over time (Figure 4). Importantly, in contrast to the uniformly spread-out cells detected on the flat surface, the cells on the G1 surface exhibited cobblestone-like patterns that resembled the morphology of HUVECs *in vivo*.

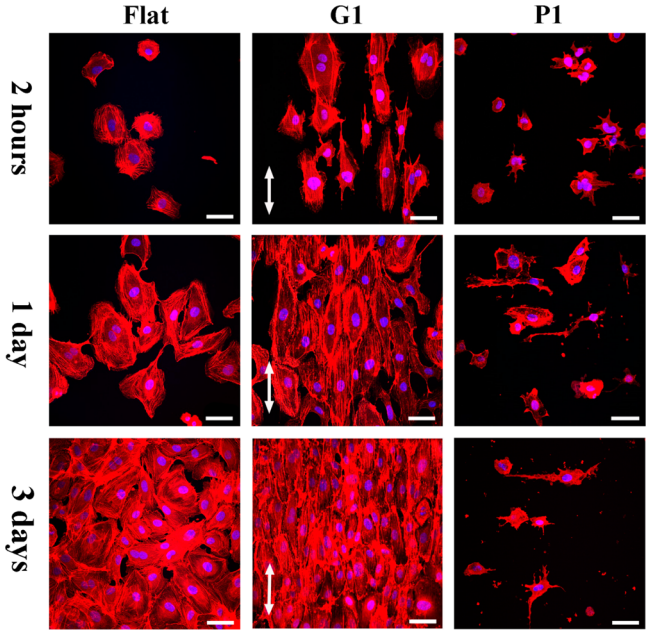


**Figure 4.** Morphology of ECs over time on the surfaces of Flat, G1, and P1 revealed by immunofluorescence staining of cytoskeletal F-actin (red) and nuclei (DAPI, blue). The arrows denote the direction of the grooves. Scale bars: 50 $\mu$m.

Fluorescence imaging also revealed a change in the shape of HUVECs cultured on the various patterns. A reduction in the minor/major axis ratio of cells on the grooves (except on the G50 surface) indicated cell elongation compared with that on the flat surface, whereas an increase in this ratio on most of the pillars reflected that the cells on this surface were more spherical than they were on the flat surface (Figure 2D). The distribution of cell-alignment angles is illustrated by a polarization graph: Figure 2E shows strong cell polarization along the direction of grooves (at 0°), in sharp contrast to the random and uniform distribution of cell-alignment angles on the pillars and on the flat surface. To further test the efficiency of contact guidance in a groove-size dependent manner, the mean values of absolute cell-alignment angles were calculated (Figure S3C), which demonstrated that contact guidance was significantly more efficient on middle-sized grooves (G10) than it was on the other grooves.

In addition, HUVECs showed a good viability on all patterned surfaces as well as on flat surfaces with minimal signs of dead/dying cells (Figures 5A and S4). More than 95% of adherent cells were alive on all surfaces tested (Figure 5B). But the level of cell viability on the G1 surface was significantly higher than that on the P1 surface, which might be responsible for the sharp difference in cell proliferation on these two surfaces.

*3.2.2. Focal Adhesion Studies.* FAs serve as cell cytoskeleton−matrix connections and may mediate cell spreading, differentiation, migration, and apoptosis.[20−22] FAs are typically classified into two categories: nascent adhesions (small, dotlike adhesions) and mature adhesions (large, elongated adhesions).[20] Figure 6A shows several mature adhesions (arrowheads) randomly distributed in a cell cultured on the flat surface; these mature adhesions reside at the ends of stress fibers and follow them as the cells elongate. Furthermore, numerous nascent adhesions (arrows) were concentrated at the lamellipodia present on the cell's leading edges on the flat

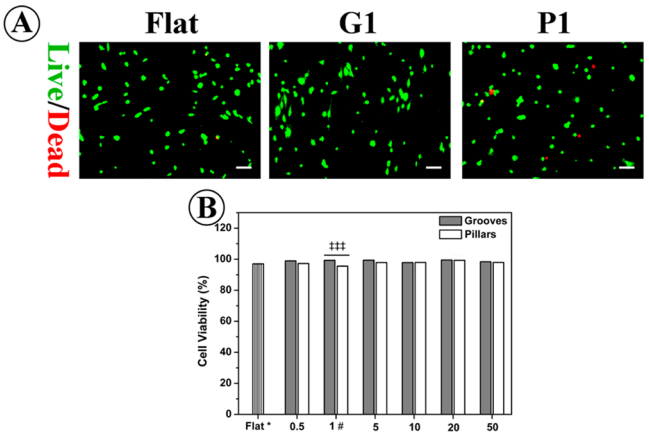


**Figure 5.** Effects of topographic patterns on EC viability. (A) Live cells (green) and dead cells (red) on the surfaces of Flat, G1, and P1. Scale bars: 100 $\mu$m. (B) Quantification of cell viability on various patterned surfaces, which was analyzed from at least nine images of each patterned motif. Statistically significant differences are marked as follows: ‡ same-sized groove vs pillar.

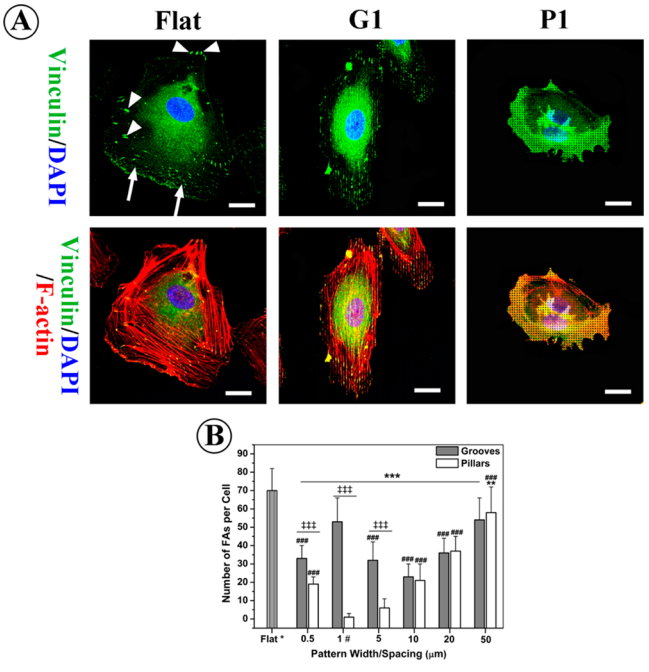


**Figure 6.** Effects of topographic patterns on FA formation. (A) Immunostaining of vinculin (green), F-actin (red), and nuclei (DAPI, blue). Scale bars: 20 $\mu$m. (B) Number of FAs per cell on various patterned surfaces. Statistically significant differences are marked as follows: * vs flat surface; # vs G1 for grooves or P1 for pillars; ‡ same-sized groove vs pillar.

surface. By contrast, FAs in cells on the G1 surface were prevalent at both the leading and trailing edges and were predominantly elongated and aligned along the groove direction, together with stress fibers. However, the degree of FA elongation and alignment was greatly diminished when the groove size was increased to 5 $\mu$m or larger (Figure S5). Moreover, the width of the FAs was dictated, as expected, by the width of the ridges on the underlying substrate in the case of small-sized grooves (G0.5 and G1), because FAs are the interaction sites between cells and substrates (the ridges in this case). Strikingly, on the P1 surface, FA formation was almost eliminated and we only observed cytosolic vinculin, which was inactive and was not recruited to FAs; however, FAs were detected around the periphery of cells on the P0.5 surface (Figure S5). Furthermore, the number of FAs per cell was quantified (Figure 6B). The pillars displayed a typical biphasic dependency on pillar size, decreasing from P50 (58 FAs/cell) to P1 (1 FA/cell) and then increasing on the P0.5 surface (19 FAs/cell). By comparison, considerably more FAs were observed on the G1 surface (53 FAs/cell) and the flat surface (69 FAs/cell). Notably, in contrast to the absence of stress fiber on the P1 surface, the flat surface induced numerous bundles of stress fiber with random orientation, and the G1 surface induced strongly orientated stress fibers.

*3.2.3. Cell Phenotype.* Cells including endothelial cells may lose tissue-specific traits when cultured *in vitro*.[23] To determine the phenotypes of HUVECs under our culture conditions, we analyzed the expression of two endothelial cell markers: platelet endothelial cell adhesion molecule (PECAM-1/CD31) and von Willebrand factor (vWF). CD31 functions as a cell−cell adhesion protein by mediating the homophilic binding of endothelial cells and is therefore crucial for endothelial cell monolayer formation and vascular integrity.[24] Conversely, vWF is a multimeric plasma glycoprotein expressed specifically by endothelial cells and megakaryocytes, and vWF is stored in the Weibel-Palade bodies of endothelial cells.[25]

As shown in Figure 7A, CD31 was distributed on the entire plasma membrane of HUVECs and concentrated at the

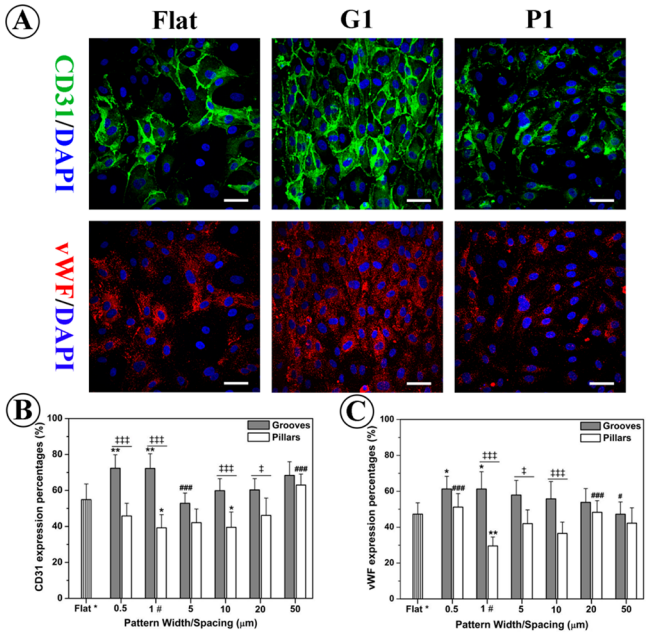


**Figure 7.** Effects of topographic patterns on EC phenotype. (A) Immunostaining of CD31 (green), vWF (red) and nuclei (DAPI, blue). Scale bars: 50 $\mu$m. Quantitation of relative expression of (B) CD31 and (C) vWF (cells with positive CD31 or vWF staining/total cell number). Statistically significant differences are marked as follows: * vs flat surface; # vs G1 for grooves or P1 for pillars; ‡ same-sized groove vs pillar.

intercellular junctions of the cells cultured on the G1 surface, agreeing well with previous observations.[26] By contrast, substantially less CD31 was expressed in the cells on the flat surface, CD31 was restricted to a small region of single cells, and the cells exhibited less intercellular adhesions on the P1

surface. The relative expression of CD31 on the various patterned surfaces was quantified (Figure 7B): the highest CD31 expression (~72%) was observed on the G1 and G0.5 surfaces, and the lowest on the P1 surface (~39%). These results suggested that the formation and maturation of stable cell−cell contacts were promoted by the small-sized grooves but were strongly suppressed by the small-sized pillars.

A punctate labeling of vWF was clearly detected and vWF was widely distributed within the cytoplasm of HUVECs cultured on the G1 and the flat surfaces (Figure 7A). By contrast, vWF was only clustered at the perinuclear region of the cells on the P1 surface. Consistent with this result, quantitation (Figure 7C) suggested that cells cultured on the small-sized grooves (G1 and G0.5) showed the highest vWF expression, whereas those on the P1 exhibited the lowest expression. These findings further demonstrated that the small-sized grooves (i.e., G1 and G0.5) promoted better endothelial phenotype of HUVECs than other topographic features did.

**3.3. HUASMCs Growth.** Figure 8 shows the typical growth of HUASMCs after culturing for 1 day and 3 days. HUASMCs

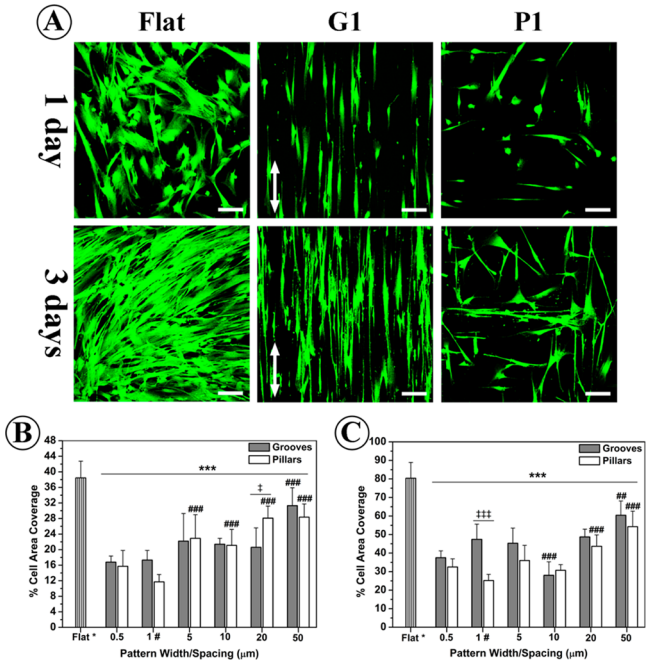


**Figure 8.** (A) Growth of SMCs over time on the surfaces of Flat, G1, and P1 revealed by immunofluorescence staining with $\alpha$-SMA. The arrows denote direction of grooves. Scale bars: 100 $\mu$m. Quantitative analysis of area coverage by SMCs on various patterned surfaces after culturing for (B) 1 day and (C) 3 days. Statistically significant differences are marked as follows: * vs flat surface; # vs G1 for grooves or P1 for pillars; ‡ same-sized groove vs pillar.

cultured on the flat surface displayed an epithelioid/rhomboid morphology after 1 day in culture and typical hill-and-valley growth patterns after 3 days in culture, which resembled the proliferative phenotype of SMCs.[27] By contrast, SMCs cultured on the grooves showed an elongated, spindle-shaped morphology and the cells aligned uniformly along the direction of the grooves, which resembled their native morphology and their organization *in vivo* (Figures 8A and S6). Most SMCs cultured on pillars (especially small-sized pillars), however, exhibited a less-spread, elongated morphology and were preferentially orientated parallel to either the rows or columns of pillars. These results suggested that the pillars nonselectively suppressed SMC spreading, as they did in the case of HUVECs. Figure 9 shows SEM micrographs of HUASMCs, which further

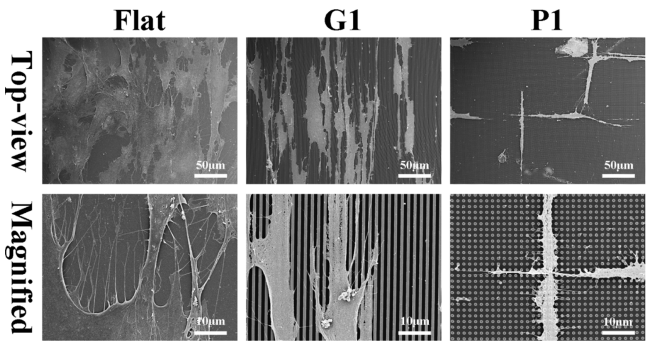


**Figure 9.** Top-view and magnified top-view of the SEM images of SMCs on the surfaces of Flat, G1, and P1 after culturing for 1 day.

confirmed the results presented in Figure 8A. SMCs cultured on the flat surface exhibited a proliferative-like phenotype featuring a randomly spread-out morphology and well-formed cell−cell adhesions. SMC spreading on the G1 surface appeared to be restricted in the direction perpendicular to the grooves, where cells were more isolated than in other places and were mostly parallel to one another, which suggested a contractile phenotype. SMCs exhibited orthogonal-type growth on the P1 surface, and the cell grew along two perpendicular directions, either along the rows or the columns of pillar arrays.

We quantified the coverage by SMCs on various patterned surfaces to measure cell growth (Figure 8B and C). After 1 day in culture, the area covered by cells was substantially lower on all the patterned surfaces, especially on small-sized patterns (e.g., ~17% coverage on G1, and ~11% on P1), as compared with the ~38% coverage on the flat surface. After 3 days in culture, ~80% area of the flat surface was covered by SMCs, which was 1.7-times and 3.2-times larger than that measured for the G1 and P1 surfaces, respectively. Note that the G1 surfaces showed higher levels of relative increase in cell area coverage from day 1 to 3, comparing with either the flat surface or P1 surface (Figure S7). However, the G10 and P10 surfaces showed much lower levels of increase from day 1 to 3. It is noteworthy that the cell area coverage on the flat surface might be underestimated as a result of multilayered growth of densely populated SMCs, so that we conclude that both the grooves and pillars effectively inhibited the spreading and proliferation of SMCs compared to the flat surface.

**3.4. Platelet Adhesion.** Next, we analyzed platelet adhesion and activation after culturing for 2 h (Figure 10). The morphologies of adherent platelets are classified into five stages from the lowest to the highest levels of activation: round, dendritic, spread dendritic, spreading, and fully spreading, as illustrated in Figure 10B.[28] Our experiments showed that the G1 and P1 surfaces reduced platelet adhesion and especially platelet activation. Almost all platelets adhered on the G1 and P1 surfaces remained spherical and separated and displayed considerably fewer pseudopodia than they did on other surfaces, whereas numerous platelets adhered on the flat surface and most of them were in the fully spreading state.

Quantitative analysis indicated that the number of adherent platelets was 26% lower on the G1 and 37% lower on the P0.5 and P1 surfaces than that on the flat surface; however, the number of adherent platelets on patterns of other sizes was

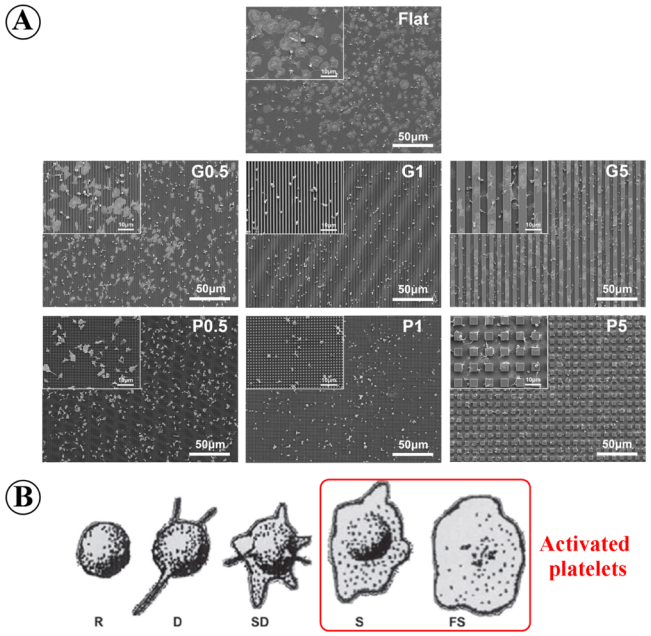


**Figure 10.** (A) SEM images of adherent platelets on various patterned surfaces after culturing for 2 h in PRP. (B) Typical morphology of adhernt platelets, R, round; D, dendtritic; SD, spreading dendritic; S, spreading; FS, fully spreading. Platelets with F and FS were charactrized as activited platelets.

comparable to that on the flat surface (Figure 11A). The percentage of activated platelets was calculated by quantifying

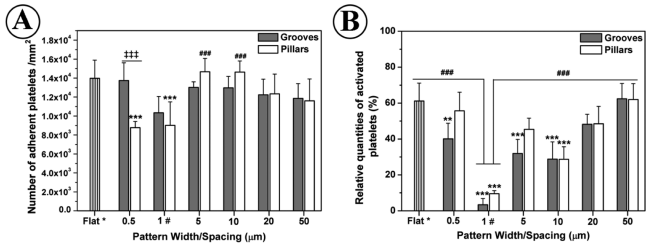


**Figure 11.** (A) Quantitative analysis of number of adherent platelets on various surfaces, which were analyzed from at least five random SEM images at 500× magnification. (B) Quantitative analysis of relative quantification of activated platelets (number of platelets with spreading or fully spreading morphology/total number of adherent platelets) on various surfaces. Statistically significant differences are marked as follows: * vs flat surface; # vs G1 for grooves or P1 for pillars; ‡ same-sized groove vs pillar.

the platelets exhibiting spreading and fully spreading morphologies, which is the method typically used to identify activated platelets.[29,30] The G1 and P1 surfaces drastically reduced the percentage of activated platelets, to 3% and 9%, respectively, from 61% on the flat surface (Figure 11B). With both the groove and pillar pattern geometries, the percentage of activated platelets showed a characteristic biphasic dependency on pattern size: the percentage was lowest on 1 μm sized patterns, but it was markedly higher when the patterns were either smaller or larger.

## 4. DISCUSSION

The quest for the ideal vascular stents has aroused great interest in the development of multifunctional biomaterials with capability of promoting endothelialization and concurrently inhibiting both SMC proliferation and platelet adhesion. Recently, a few chemical cues incorporated into biomaterials have shown targeted multifunctionality of vascular stents.[19,31] To date, however, it has been not clear if the micro/nanostructure of the cell adhesion substratum can be an instructive cue selectively directing the fates of ECs, SMCs, and platelets. To elucidate this question, we developed a novel patterned platform featuring multimotifs of topographic patterns, which is demonstrated to be a highly effective protocol for studying how ECs, SMCs, and platelets responded to various topographies. The findings argue that the topography of the cell adhesion substratum can indeed selectively direct the fates of ECs, SMCs, and platelets. Subtle changes in topographic geometries and feature sizes profoundly influenced the behaviors of vascular cells and platelets.

The experimental results suggested that grooves seemed to induce vascular cell selectivity, whereas pillars were non-selectively "antiproliferative". We observed higher proliferation rates of ECs on the 1−5 μm grooves but remarkably lower rates on 1−5 μm pillars compared with the proliferation rates on other surfaces (Figure 2B). Moreover, the enhanced expression of endothelial cell markers (CD31 and vWF) of the ECs cultured on grooves reinforced the argument that grooves provide a more favorable microenvironment for rapid endothelialization than the pillars and the flat surface do. Furthermore, we found both grooves and pillars did not support SMC growth well compared with the flat surface (Figure 8). The spindle-shaped appearance of SMCs and their isolated cell−cell interactions might suggest contractile phenotype induced by grooves and pillars. Overall, the results indicate that selectively directing of vascular cell fates can indeed be instructed by the geometry of topography in the cell environment.

Apart from topographic geometry, the fates of vascular cells and platelets are exquisitely sensitive to topographic size. Identifying the optimal topography that induces desired responses of vascular cells and platelets has been not only fundamentally important for understanding cell−surface interaction, but also practically important for development multifunctional vascular stents. In this study, pattern sizes ranging from submicrometer to tens of micrometers were used to clearly demonstrate that a narrow window of pattern sizes existed (0.5−5 μm) within which subtle changes in the pattern size profoundly influenced the adhesion, morphology, proliferation, and FA development of ECs. Particularly, ECs were substantially more sensitive to pattern-size change on pillars than on grooves. Importantly, we identified a characteristic size of around 1 μm that maximally induced the geometric effects of the patterns, while, with either pattern size increasing or decreasing, the topographic effects on EC faded out. Moreover, the disparity in the responses of ECs cultured on grooves and pillars also maximized at a size of 1 μm and gradually diminished with either an increase or a decrease in pattern size. Notably, the inhibitory effects of various patterns on SMCs displayed a similar biphasic dependence on pattern sizes, but differing from EC the 10 μm grooves and pillars seemed to induce lower growth rate of SMCs than 1 μm grooves and pillars. This may be ascribed to 10 μm patterns providing more severe restriction to SMC growth than 1 μm patterns, as the size of SMC is larger than EC. In addition to the size effects observed on vascular cells, we found that patterns also affected platelets. Our previous study indicated that 0.5 μm grooves

would enhance platelet adhesion and activation compared to either flat surface or 0.5 $\mu$m pillars,[5] which was consistent with the current study. In this study, it was interesting to find that adherent platelets on 1 $\mu$m grooves or pillars exhibited substantially lower activation levels than on other sizes of patterns or on the flat surface. This may suggest that platelet adhesion may be more sensitive to pattern size than to pattern geometry that we have studied. Therefore, we propose an optimized topography of 1 $\mu$m sized groove for targeted multifunctionality: EC growth was favored, whereas SMC proliferation and platelet adhesion/activation were inhibited.

The further question that should be answered is this: what are the mediators for selectively directing vascular cell and platelet fates? It has been suggested that changes in cell shape and cell area produce alternation of vascular cell functions and phenotypes by regulating cytoskeletal reorganizations.[6,32,33] In this study, we indeed found that FA assembly and actin stress fiber development, defining the cytoskeletal organization and cell shape, were differentially regulated by various topographies. The 1 $\mu$m grooves induced large amount of elongated FAs and stress fibers with strong orientation in ECs, which subsequently defines the well-organized cytoskeleton and elongated cell shape. Similarly, the grooves also induced the strongly elongated cell shape of SMCs. This bipolar, elongated shape in both ECs and SMCs makes these cells resemble their in-vivo-like states, which may be responsible for selective effects of grooves on the growth of ECs and SMCs. By contrast, assembly of FAs and stress fibers vanished in ECs on 1 $\mu$m pillars, which might give rise to disorganized cytoskeleton and suppressed cell spreading. Similarly, the pillars also suppressed the spreading and growth of SMCs. We herein speculate that strong spatial confinement in multiple directions of the pillars hinders cellular growth and may account for its nonselectively "antiproliferative" effect. Furthermore, only the 1 $\mu$m grooves and pillars potently inhibited platelet adhesion and activation. This might result from the potential reduction in effective platelet contact area on 1 $\mu$m patterns, which have a size comparable to the diameter of platelets (1−2 $\mu$m).[5,14]

## 5. CONCLUSIONS

The patterned platform featuring 12 topographic motifs in a single substrate enables us to efficiently assess vascular cell selectively and hemocompatibility. Using this patterned platform, we revealed that surface topography can selectively direct the fates of vascular cells and platelets. Importantly, our study results indicate that the 1 $\mu$m groove is the most favorable topography for improving the endothelial cell attachment, proliferation, and functions by regulating focal adhesion assembly and cytoskeleton development. Furthermore, both grooves and pillars could suppress the smooth muscle cell spreading and growth. Notably, the grooves and pillars at 1 $\mu$m size effectively reduce platelet adhesion and activation. The good vascular cell selectivity and hemocompatibility induced by topographic patterns provide a promising direction for further research and development of vascular devices. The study also reveals the pillar pattern's nonselective inhibition of cell growth, which might make it an "antiproliferative" topographic feature for certain applications.

## ■ ASSOCIATED CONTENT

### Supporting Information

(1) The cell density of ECs on the surfaces after culturing cells for 1 and 3 days; (2) fluorescence images of EC morphology on various pattered surfaces; (3) quantitative analysis of EC morphology on various patterned surfaces; (4) EC viability on various patterned surfaces; (5) fluorescence images of FA development on the surfaces of G0.5, P0.5, and P5; (6) fluorescence images of SMC growth over time on various patterned surfaces; (7) the relative increase in cell area coverage of SMCs on various patterned surfaces from 1 to 3 days; (8) SEM images of adherent platelets on various patterned surfaces. This material is available free of charge via the Internet at http://pubs.acs.org.

## ■ AUTHOR INFORMATION

### Corresponding Author

*E-mail: meleng@ust.hk.

### Notes

The authors declare no competing financial interest.

## ■ ACKNOWLEDGMENTS

This work was financially supported by the Research Grants Council of Hong Kong (FSGRF13EG58), Program for New Century Excellent Talents in University (NCET-10-0704), and Sichuan Youth Science Technology Foundation (2011JQ0010). Samples were characterized at the Materials Characterization and Preparation Facility (MCPF) and the Nanoelectronics Fabrication Facility (NFF) at the Hong Kong University of Science and Technology (HKUST).

## ■ REFERENCES

(1) Bettinger, C. J.; Langer, R.; Borenstein, J. T. Engineering Substrate Topography at the Micro- and Nanoscale to Control Cell Function. *Angew. Chem., Int. Ed.* **2009**, *48*, 5406−5415.

(2) Liliensiek, S. J.; Wood, J. A.; Yong, J.; Auerbach, R.; Nealey, P. F.; Murphy, C. J. Modulation of Human Vascular Endothelial Cell Behaviors by Nanotopographic Cues. *Biomaterials* **2010**, *31*, 5418−5426.

(3) Huang, N. F.; Lai, E. S.; Ribeiro, A. J. S.; Pan, S.; Pruitt, B. L.; Fuller, G. G.; Cooke, J. P. Spatial Patterning of Endothelium Modulates Cell Morphology, Adhesiveness and Transcriptional Signature. *Biomaterials* **2013**, *34*, 2928−2937.

(4) Lu, J.; Rao, M. P.; MacDonald, N. C.; Khang, D.; Webster, T. J. Improved Endothelial Cell Adhesion and Proliferation on Patterned Titanium Surfaces with Rationally Designed, Micrometer to Nanometer Features. *Acta Biomater.* **2008**, *4*, 192−201.

(5) Zorlutuna, P.; Rong, Z.; Vadgama, P.; Hasirci, V. Influence of Nanopatterns on Endothelial Cell Adhesion: Enhanced Cell Retention under Shear Stress. *Acta Biomater.* **2009**, *5*, 2451−2459.

(6) Thakar, R. G.; Cheng, Q.; Patel, S.; Chu, J.; Nasir, M.; Liepmann, D.; Komvopoulos, K.; Li, S. Cell-Shape Regulation of Smooth Muscle Cell Proliferation. *Biophys. J.* **2009**, *96*, 3423−3432.

(7) Thakar, R. G.; Ho, F.; Huang, N. F.; Liepmann, D.; Li, S. Regulation of Vascular Smooth Muscle Cells by Micropatterning. *Biochem. Biophys. Res. Commun.* **2003**, *307*, 883−890.

(8) Sarkar, S.; Dadhania, M.; Rourke, P.; Desai, T. A.; Wong, J. Y. Vascular Tissue Engineering: Microtextured Scaffold Templates to Control Organization of Vascular Smooth Muscle Cells and Extracellular Matrix. *Acta Biomater.* **2005**, *1*, 93−100.

(9) Csaderova, L.; Martines, E.; Seunarine, K.; Gadegaard, N.; Wilkinson, C. D. W.; Riehle, M. O. A Biodegradable and Biocompatible Regular Nanopattern for Large-Scale Selective Cell Growth. *Small* **2010**, *6*, 2755−2761.

(10) Dalby, M. J.; Riehle, M. O.; Johnstone, H.; Affrossman, S.; Curtis, A. S. G. In Vitro Reaction of Endothelial Cells to Polymer Demixed Nanotopography. *Biomaterials* **2002**, *23*, 2945−2954.

(11) Dickinson, L. E.; Rand, D. R.; Tsao, J.; Eberle, W.; Gerecht, S. Endothelial Cell Responses to Micropillar Substrates of Varying

Dimensions and Stiffness. *J. Biomed. Mater. Res., Part A* **2012**, *100 A*, 1457−1466.
(12) Milner, K. R.; Snyder, A. J.; Siedlecki, C. A. Sub-Micron Texturing for Reducing Platelet Adhesion to Polyurethane Biomaterials. *J. Biomed. Mater. Res., Part A* **2006**, *76*, 561−570.
(13) Koh, L. B.; Rodriguez, I.; Venkatraman, S. S. The Effect of Topography of Polymer Surfaces on Platelet Adhesion. *Biomaterials* **2010**, *31*, 1533−1545.
(14) Ding, Y.; Leng, Y.; Huang, N.; Yang, P.; Lu, X.; Ge, X.; Ren, F.; Wang, K.; Lei, L.; Guo, X. Effects of Microtopographic Patterns on Platelet Adhesion and Activation on Titanium Oxide Surfaces. *J. Biomed. Mater. Res., Part A* **2013**, *101 A*, 622−632.
(15) Yang, J.; Rose, F. R. A. J.; Gadegaard, N.; Alexander, M. R. A High-Throughput Assay of Cell-Surface Interactions Using Topographical and Chemical Gradients. *Adv. Mater.* **2009**, *21*, 300−304.
(16) Reynolds, P. M.; Pedersen, R. H.; Riehle, M. O.; Gadegaard, N. A Dual Gradient Assay for the Parametric Analysis of Cell-Surface Interactions. *Small* **2012**, *8*, 2541−2547.
(17) Unadkat, H. V.; Hulsman, M.; Cornelissen, K.; Papenburg, B. J.; Truckenmulüler, R. K.; Post, G. F.; Uetz, M.; Reinders, M. J. T.; Stamatialis, D.; Van Blitterswijk, C. A.; De Boer, J. An Algorithm-Based Topographical Biomaterials Library to Instruct Cell Fate. *Proc. Natl. Acad. Sci. U.S.A.* **2011**, *108*, 16565−16570.
(18) Urquhart, A. J.; Anderson, D. G.; Taylor, M.; Alexander, M. R.; Langer, R.; Davies, M. C. High Throughput Surface Characterisation of a Combinatorial Material Library. *Adv. Mater.* **2007**, *19*, 2486−2491.
(19) Yang, Z.; Tu, Q.; Wang, J.; Huang, N. The Role of Heparin Binding Surfaces in the Direction of Endothelial and Smooth Muscle Cell Fate and Re-Endothelialization. *Biomaterials* **2012**, *33*, 6615−6625.
(20) Parsons, J. T.; Horwitz, A. R.; Schwartz, M. A. Cell Adhesion: Integrating Cytoskeletal Dynamics and Cellular Tension. *Nat. Rev. Mol. Cell Biol.* **2010**, *11*, 633−643.
(21) Yu, H.; Lui, Y. S.; Xiong, S.; Leong, W. S.; Wen, F.; Nurkahfianto, H.; Rana, S.; Leong, D. T.; Ng, K. W.; Tan, L. P. Insights into the Role of Focal Adhesion Modulation in Myogenic Differentiation of Human Mesenchymal Stem Cells. *Stem Cells Dev.* **2013**, *22*, 136−147.
(22) Kim, D. H.; Wirtz, D. Focal Adhesion Size Uniquely Predicts Cell Migration. *FASEB J.* **2013**, *27*, 1351−1361.
(23) Müller, A. M.; Hermanns, M. I.; Skrzynski, C.; Nesslinger, M.; Müller, K.-M.; Kirkpatrick, C. J. Expression of the Endothelial Markers Pecam-1, Vwf, and Cd34 in Vivo and in Vitro. *Exp. Mol. Pathol.* **2002**, *72*, 221−229.
(24) Albelda, S. M.; Muller, W. A.; Buck, C. A.; Newman, P. J. Molecular and Cellular Properties of Pecam-1 (Endocam/Cd31): A Novel Vascular Cell-Cell Adhesion Molecule. *J. Cell Biol.* **1991**, *114*, 1059−1068.
(25) Mannucci, P. M. Platelet Von Willebrand Factor in Inherited and Acquired Bleeding Disorders. *Proc. Natl. Acad. Sci. U.S.A.* **1995**, *92*, 2428−2432.
(26) Scholz, D.; Schaper, J. Platelet/Endothelial Cell Adhesion Molecule-1 (Pecam-1) Is Localized over the Entire Plasma Membrane of Endothelial Cells. *Cell Tissue Res.* **1997**, *290*, 623−631.
(27) Powell, R. J.; Cronenwett, J. L.; Fillinger, M. F.; Wagner, R. J.; Sampson, L. N. Endothelial Cell Modulation of Smooth Muscle Cell Morphology and Organizational Growth Pattern. *Ann. Vasc. Surg.* **1996**, *10*, 4−10.
(28) Goodman, S. L.; Grasel, T. G.; Cooper, S. L.; Albrecht, R. M. Platelet Shape Change and Cytoskeletal Reorganization on Polyurethaneureas. *J. Biomed. Mater. Res.* **1989**, *23*, 105−123.
(29) Aslan, J. E.; Itakura, A.; Gertz, J. M.; McCarty, O. J. T. Platelet Shape Change and Spreading. *Methods Mol. Biol.* **2012**, *788*, 91−100.
(30) Jones, M. I.; McColl, I. R.; Grant, D. M.; Parker, K. G.; Parker, T. L. Protein Adsorption and Platelet Attachment and Activation, on Tin, Tic, and Dlc Coatings on Titanium for Cardiovascular Applications. *J. Biomed. Mater. Res.* **2000**, *52*, 413−421.
(31) Hoshi, R. A.; Van Lith, R.; Jen, M. C.; Allen, J. B.; Lapidos, K. A.; Ameer, G. The Blood and Vascular Cell Compatibility of Heparin-Modified Eptfe Vascular Grafts. *Biomaterials* **2013**, *34*, 30−41.
(32) Cha, K. J.; Hong, J. M.; Cho, D. W.; Kim, D. S. Enhanced Osteogenic Fate and Function of Mc3t3-E1 Cells on Nanoengineered Polystyrene Surfaces with Nanopillar and Nanopore Arrays. *Biofabrication* **2013**, *5*, 025007.
(33) Versaevel, M.; Grevesse, T.; Gabriele, S. Spatial Coordination between Cell and Nuclear Shape within Micropatterned Endothelial Cells. *Nat. Commun.* **2012**, *3*, 671.